The Journal of Chemical Physics

RESEARCH ARTICLE | AUGUST 23 2022

# Local charge-displacement analysis: Targeting local charge-flows in complex intermolecular interactions

G. Nottoli ; B. Ballotta ; S. Rampino



*J. Chem. Phys.* 157, 084107 (2022)
https://doi.org/10.1063/5.0095142









AIP Publishing

The Journal of Chemical Physics ARTICLE scitation.org/journal/jcp

# Local charge-displacement analysis: Targeting local charge-flows in complex intermolecular interactions

Cite as: J. Chem. Phys. 157, 084107 (2022); doi: 10.1063/5.0095142
Submitted: 8 April 2022 • Accepted: 28 July 2022 •
Published Online: 23 August 2022



G. Nottoli, B. Ballotta, and S. Rampino[a),b)]

## AFFILIATIONS

Scuola Normale Superiore, Piazza dei Cavalieri 7, 56126 Pisa, Italy

**Note:** This paper is part of the JCP Special Topic on Nature of the Chemical Bond.
[a)]**Author to whom correspondence should be addressed:** sergio.rampino@unipd.it
[b)]**Present address:** Università degli Studi di Padova, Dipartimento di Scienze Chimiche, Via Marzolo 1, 35131 Padova, Italy.
**Also at:** Istituto Nazionale di Fisica Nucleare, Sezione di Pisa, Largo Bruno Pontecorvo 3, 56127 Pisa, Italy.

## ABSTRACT

Charge-displacement (CD) analysis has recently proven to be a simple and powerful scheme for quantitatively analyzing the profile the charge redistribution occurring upon intermolecular interactions along a given interaction axis. However, when two molecular fragments bind through complex interactions involving multiple concurrent charge flows, ordinary CD analysis is capable of providing only an averaged picture of the related charge-flow profiles and no detailed information on each of them. In this article, we combine CD analysis with a Hirshfeld partitioning of the molecular charge redistribution for a local analysis on focused portions of the molecule, allowing for a detailed characterization of one charge flow at a time. The resulting scheme—the local charge-displacement (LCD) analysis—is tested on the intriguing case of the dimethyl sulfide–sulfur dioxide complex, characterized by concurrent charge flows relating to a sulfur–sulfur homochalcogen interaction and a pair of hydrogen bonds. The LCD scheme is then applied to the analysis of multiple hydrogen bonding in the acetic acid dimer, of base-pairing interactions in DNA, and of ambifunctional hydrogen bonding in the ammonia–pyridine complex.



## I. INTRODUCTION

Since Lewis's original work on electron-pair sharing in 1916,[1] chemical bonding is commonly associated with a redistribution of the electrons around the involved atoms. While in Lewis's diagrams the electrons are schematically depicted as dots and lines, modern electronic-structure calculations coupled to state-of-the-art molecular graphics make it possible to effectively model, visualize, and analyze the redistribution of electron clouds within a full quantum mechanical framework. In fact, as shown by the pioneering works of Bader on diatomics in his late-60s works,[2,3] a static picture of the electron-charge redistribution occurring upon chemical bonding can be conveniently obtained by computing a suitably formulated electron-density difference between a bound adduct and its unbound fragments, thus obtaining a three-dimensional function $\Delta\rho(\boldsymbol{r})$, with $\boldsymbol{r} \equiv (x, y, z)$, that is negative in regions of electron depletion and positive in regions of electron accumulation. This electron-density difference is typically obtained by subtracting from the electron density of an adduct AB that of a "reference," unbound system made up of a superposition of the densities of the two constituent (non-interacting) fragments A and B frozen at their in-adduct geometries,

$$\Delta\rho(\boldsymbol{r}) = \rho^{\mathrm{AB}}(\boldsymbol{r}) - \left[\rho^{\mathrm{A}}(\boldsymbol{r}) + \rho^{\mathrm{B}}(\boldsymbol{r})\right]. \tag{1}$$

A visual analysis of $\Delta\rho(\boldsymbol{r})$ often offers remarkable qualitative insight into the nature of the chemical bond at hand. For the purpose of quantitative analysis, however, it is convenient to compact such three-dimensional information into a more manageable lower-dimensionality function. Accordingly, if a privileged axis can be recognized as the one along which the intermolecular interaction develops, a one-dimensional "profile" of the overall charge redistribution along this interaction axis—which we shall notate as $z$—can be computed by means of the following integration:

$$\Delta\rho(z) = \int_{-\infty}^{\infty}\int_{-\infty}^{\infty} \Delta\rho(x, y, z)\, \mathrm{d}x\, \mathrm{d}y. \tag{2}$$

The information conveyed by Eq. (2) can be recast in a more convenient form by performing the following progressive integration:

$$\Delta q(z) = \int_{-\infty}^{z} \Delta\rho(z')\, dz' \tag{3}$$

which, by definition, quantifies at any point $z$ the exact amount of electron charge that, upon the fragment–fragment interaction, has moved from right to left [or from left to right, for negative values of $\Delta q(z)$] across a plane perpendicular to the interaction axis through the $z$ point. These two functions are the analog of the planar density and electron count function, respectively, defined by Brown and Shull[4,5] by integration of $\rho(\boldsymbol{r})$ rather than $\Delta\rho(\boldsymbol{r})$. The second function [Eq. (3)], in particular, is the so-called charge-displacement (CD) function first introduced in Ref. 6 to study the chemical bond between gold and the noble gases, and providing, as already mentioned, a $z$-resolved quantitative picture of the charge transfer associated with the intermolecular interaction (see also Chap. 14 of Ref. 7 for an introduction to CD analysis).

In spite of being very simple in its formulation, the CD function has proven to be a versatile tool for the analysis of intermolecular interactions, especially when combined with the Natural Orbitals for Chemical Valence in the so-called NOCV-CD scheme.[8,9] It has, in fact, offered remarkable qualitative and quantitative insight into coordination bonding of organometallic complexes[10–13] and in the context of more elusive, including non-covalent, interactions.[14–19] Moreover, CD analysis has been recently generalized on one hand to the case of curvilinear interaction paths (leveraging on a Voronoi tessellation technique),[20] and on the other hand to the fully relativistic framework[9,21,22] for the analysis of charge redistributions obtained by four-component Dirac–Kohn–Sham calculations.[23,24]

CD analysis, however, has an intrinsic limitation, which arises from its own peculiar formulation and prevents one from applying it to a potentially important class of systems. In particular, it inescapably fails to properly characterize complex intermolecular interactions where there are multiple bonding pairs and, thus, several associated concurrent charge flows running in parallel between the fragments. Consider, for instance, the dimethyl sulfide (DMS)–sulfur dioxide ($SO_2$) complex depicted in Fig. 1 and featuring a sulfur–sulfur homochalcogen interaction (yellow dashed line) and a pair of concurrent hydrogen bonds (gray dashed lines).

In this case, due to its peculiar formulation, the integration of Eqs. (2) and (3) returns information on the overall charge flow along $z$, resulting from all three interactions, thus providing an "averaged" picture of these interactions and no detailed information on each of them.

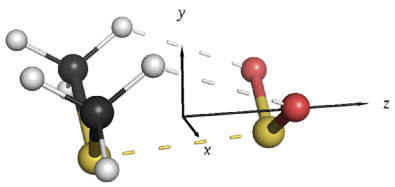


**FIG. 1.** Sulfur–sulfur homochalcogen interaction and hydrogen bonds in the DMS–$SO_2$ complex.

The purpose of this work is to illustrate a novel strategy for overcoming the above outlined shortcomings by devising a scheme for a "local" analysis of charge flows on focused portions of a molecular system. The scheme—the local charge-displacement (LCD) analysis—is based on a Hirshfeld partitioning[25] of the electron-charge redistribution and allows for a decomposition of the overall redistribution into additive terms localized in relevant molecular regions and relating to the different charge flows. Accordingly, the article is structured as follows: In Sec. II, the method is described. Section III summarizes the computational details adopted for the reported calculations. In Sec. IV, LCD analysis is performed on the above-mentioned DMS–$SO_2$ complex and the features of the method are discussed in relation to the obtained results. The analysis is then extended to the case of multiple hydrogen bonding in the acetic acid dimer and in DNA base pairs, and of so-called ambifunctional hydrogen bonding in the ammonia–pyridine complex. Finally, in Sec. V, some conclusions are drawn and perspectives are outlined.

## II. LOCAL CHARGE-DISPLACEMENT ANALYSIS

With an eye on Fig. 1, essentially all we want to do is disentangle from the overall charge redistribution $\Delta\rho(\boldsymbol{r})$ upon interaction of DMS with $SO_2$, a "local" contribution relating to the S···S interaction, and two analogous local contributions relating to the two CH···O hydrogen bonds. Ideally, these three contributions, if summed up to a fourth contribution accounting for the charge redistribution around the remaining four H atoms, should yield the overall charge redistribution $\Delta\rho(\boldsymbol{r})$. In other words, we seek a decomposition of $\Delta\rho(\boldsymbol{r})$ in terms of additive local components relating to charge flows occurring around well-defined areas of the molecule. This can be easily achieved through a Hirshfeld partitioning[25] of $\Delta\rho(\boldsymbol{r})$ that, for the reader's convenience, we shall briefly review in the following. It is worth noting here that, as known, the Hirshfeld partitioning scheme has a certain degree of arbitrariness. Not only that it is not, in fact, the only possible way to partition the electron density of a molecule, but also it relies on the introduction of a reference system and on the particular choices adopted for its definition (see Ref. 26 for a critical analysis). It should thus be stressed that the methodology presented herein shares some of the criticalities of the Hirshfeld partitioning scheme, which nonetheless represents a popular and well-established interpretative tool. Refinements have been proposed to the original Hirshfeld partitioning scheme, such as the iterative Hirshfeld partitioning procedure (also known as Hirshfeld-I), which mitigate some of its shortcomings (the reader is referred to Ref. 27 for a recent interesting review on the subject). While these refined approaches can easily be integrated in our methodology, for the purpose of conveying the basic ideas of this work, it will suffice to base our discussion on Hirshfeld's original scheme.

Within Hirshfeld's partitioning scheme, a so-called promolecular electron density is defined as the superposition of all spherically averaged atomic densities centered on the atoms that make up the molecular system,

$$\rho^{\mathrm{pro}}(\boldsymbol{r}) = \sum_{i}^{N_{\mathrm{atoms}}} \rho_i^{\mathrm{at}}(\boldsymbol{r}). \tag{4}$$

This promolecular density, which *per se* has no physical meaning, refers, thus, to the density of the constituent atoms in an "unrelaxed state" prior to molecular formation. Then, a share or weight function $w_i(\boldsymbol{r})$ is defined for each atom, returning at each point in space its relative share in the promolecular density,

$$w_i(\boldsymbol{r}) = \frac{\rho_i^{\mathrm{at}}(\boldsymbol{r})}{\rho^{\mathrm{pro}}(\boldsymbol{r})}. \tag{5}$$

The several resulting overlapping weight functions are all positive and they sum up to one in every point of space. These weight functions, which are calculated on the basis of the peculiar shapes of the atomic densities, represent, thus, an efficient "chemically" grounded partitioning criterion and can be readily used to evaluate the share of atom $i$ in other quantities such as, for instance, the molecular electron density $\rho(\boldsymbol{r})$,

$$\rho_i(\boldsymbol{r}) = w_i(\boldsymbol{r})\rho(\boldsymbol{r}). \tag{6}$$

Due to the already mentioned properties of the weight functions of being positive and summing up to one in every point of space, the total electron density may thus be decomposed in additive atomic contributions as follows:

$$\rho(\boldsymbol{r}) = \sum_i \rho_i(\boldsymbol{r}) = \sum_i w_i(\boldsymbol{r})\rho(\boldsymbol{r}). \tag{7}$$

In other words, at each point in space, the molecular density is divided among the atoms of the molecule in proportion to their respective contributions to the promolecular density.

Now, the same partitioning scheme can as well be used for the electron-density difference $\Delta\rho(\boldsymbol{r})$ [rather than the electron density $\rho(\boldsymbol{r})$] for the purpose of evaluating atomic contributions to the overall charge redistribution. As a consequence, in order to extract from $\Delta\rho(\boldsymbol{r})$ a "local" contribution $\Delta\rho_I(\boldsymbol{r})$ relating to a portion of the molecule identified by a given subset $I$ of atoms, one can simply group together the related atomic weight functions as follows:

$$w_I(\boldsymbol{r}) = \sum_{i\in I} w_i(\boldsymbol{r}) \tag{8}$$

and use this quantity to "filter" the overall charge redistribution as follows:

$$\Delta\rho_I(\boldsymbol{r}) = w_I(\boldsymbol{r})\Delta\rho(\boldsymbol{r}). \tag{9}$$

Provided that the molecule is partitioned in portions $I$ in such a way that all atoms are included and each of them appears only in one of the portions, the following additivity relation holds:

$$\Delta\rho(\boldsymbol{r}) = \sum_I \Delta\rho_I(\boldsymbol{r}). \tag{10}$$

In other words, the overall charge redistribution is decomposed in terms of additive contributions describing local charge flows occurring in focused portions of the molecule, which is exactly what we were looking for in the opening of this section.

The combination of such partitioning scheme with CD analysis is straightforward. In fact, CD analysis can be easily transferred on each local $\Delta\rho_I(\boldsymbol{r})$,

$$\Delta\rho_I(z) = \int_{-\infty}^{\infty}\int_{-\infty}^{\infty} \Delta\rho_I(x,y,z)\,\mathrm{d}x\,\mathrm{d}y, \tag{11}$$

$$\Delta q_I(z) = \int_{-\infty}^{z} \Delta\rho_I(z')\,\mathrm{d}z', \tag{12}$$

with the several $\Delta q_I(z)$—provided, again, that all atoms are included in the molecular portions and that each of them only appears in one of the portions—summing up to the total CD function,

$$\Delta q(z) = \sum_I \Delta q_I(z). \tag{13}$$

Equations (11) and (12) form the basis of the LCD analysis scheme. In practice, in the LCD analysis scheme, one divides the molecular system in several relevant portions (for instance, relating to a particular interaction, such as the S···S homochalcogen interaction or the hydrogen bonds of Fig. 1), evaluates the weight function for that portion [Eq. (8)], and uses the resulting $w_I(\boldsymbol{r})$ to calculate the related contribution $\Delta\rho_I(\boldsymbol{r})$ to the overall charge redistribution $\Delta\rho(\boldsymbol{r})$ [Eq. (9)]. The weight function $w_I(\boldsymbol{r})$ in Eq. (9) ensures that focus is made only on the relevant portion of the molecule by smoothly "turning off" the information localized in the surrounding environment. Quantitative analysis can then be performed by calculating the CD functions related to these local contributions.

In order to provide the reader with a direct feeling of how LCD analysis works, in Sec. IV A of the article, we shall test the methodology on the same case that has driven the discussion so far, the DMS–$SO_2$ complex, and illustrate the features of the method on the basis of the obtained results. The analysis will then be extended in Secs. IV B and IV C to other challenging systems.

## III. COMPUTATIONAL DETAILS

The calculations reported in this article were performed using density-functional theory (DFT) with the Gaussian suite of programs (G16 Rev. C.01),[28] adopting the double-hybrid B2PLYP[29] exchange-correlation functional in conjunction with the m-aug-cc-pVTZ-*d*H[30] basis set in which *d* functions in hydrogen atoms were removed. Semiempirical dispersion contributions were taken into account by means of Grimme's D3BJ[31] model as implemented in Gaussian. The molecular geometries of the DMS–$SO_2$ complex, the DNA base pairs, and the ammonia–pyridine complex, which are provided in the supplementary material in XYZ format, were taken from Refs. 18, 32, and 33, respectively. Those of the water dimer and of the acetic acid dimer, also reported in the supplementary material in XYZ format, were obtained by geometry optimization at the above-mentioned level of theory. LCD analysis was performed on the electron-density difference between the adduct and its constituting fragments, computed as per Eq. (1) at the optimized geometry of the adduct. It is worth mentioning here that in some cases, the choice of neutral (A and B) or charged (e.g., $A^+$ and $B^-$) fragments for the construction of the reference density is not a trivial one. All of the herein considered systems pose, however, no significant problem in this respect, as the neutral fragments are the natural and most appropriate choice. Hirshfeld partitioning and numerical integration of the discretized electron-density difference and its local contributions in the form of Gaussian cube files was conducted using in-house developed software based on the CUBES library and program suite.[34]

## IV. RESULTS AND DISCUSSION

### A. The DMS–$SO_2$ complex

The DMS–$SO_2$ complex has recently been thoroughly characterized by combining rotational spectroscopy in supersonic expansion (capable of unveiling the genuine nature of non-covalent interactions in an environment free from solvation, matrix, and crystal-packing effects) and quantum-chemical calculations in Ref. 18. As shown therein, a dominant role in the binding of DMS to $SO_2$ is played by the electrostatic interaction between the negatively charged sulfur atom of DMS and the strongly positive sulfur atom of $SO_2$, and a marked charge transfer is observed between the sulfur atoms. It should thus be stressed here that the calculations on DMS–$SO_2$ reported in this article are meant to illustrate the features of the developed methodology, while a comprehensive characterization of the DMS–$SO_2$ interaction is out of the scope of the present paper. Accordingly, we will here mainly limit the discussion to the results of the LCD analysis on the complex, making reference, where opportune, to the findings reported in Ref. 18 for further comparison, and referring the interested reader to that work for further details.

#### 1. The overall charge redistribution

We will start our discussion by performing ordinary CD analysis on the DMS–$SO_2$ complex. The overall charge redistribution $\Delta\rho(\boldsymbol{r})$ upon binding of DMS to $SO_2$, computed as per Eq. (1), is shown in the left panel of Fig. 2 as a double colored electron cloud, with red color identifying electron depletion and blue color identifying electron accumulation.

As expected, the atoms most involved in the charge redistribution taking place upon formation of the complex are the S–S couple and the two CH–O groups engaged in the two hydrogen bonds. Focusing on the H–O pairs of the hydrogen bonds, electron depletion is seen to occur around the H atoms of DMS (resulting in an increase of their positive partial charge) while electron accumulation is observed on the O atoms of $SO_2$ (resulting in an increase of their negative partial charge). As to the S–S couple, instead, charge accumulation is observed in the region between the atoms, indicating electron sharing as an important part of their interaction. On the other hand, the charge redistribution around each S atom is found to be "asymmetric": While the sulfur atom of DMS mostly undergoes electron depletion, that of $SO_2$ features electron depletion on the side facing DMS and electron accumulation in the opposite (rear) side. Note that the terms "rear" and "front" will in a few occasions be used to indicate regions of space around a given atom with respect to the interaction locus.

As mentioned above, a quantitative picture of the charge-flow profile along a directional axis can be obtained via the integration of Eqs. (2) and (3). For the purpose of analyzing the interaction between DMS and $SO_2$, a natural choice for the reference frame $(x, y, z)$ to be used for that integration is that of the principal axes of inertia of the resulting complex (precisely those shown in the left panel of Fig. 2), naturally accounting for the overall three-dimensional shape of the complex. As the reader can intuitively get by inspecting Fig. 2, one of these axes, namely the $z$ one, joins the fragments through the center of mass of the adduct, while the remaining two identify a plane $xy$, which naturally adapts between the planar orientations of the two fragments. Further analysis provided in the supplementary material shows that the results of the CD analysis remain essentially unchanged if alternative definitions of the interaction axis (i.e., the normal vector of the C–S–C plane of DMS, the normal vector of the O–S–O plane of $SO_2$, and the S···S internuclear axis) are adopted.

The charge-redistribution profile along the interaction axis $z$, $\Delta\rho(z)$, and the related CD function, $\Delta q(z)$, are shown as gray dashed line and blue solid line, respectively, in the right panel of Fig. 2, where for the reader's convenience the position of the two S atoms along the $z$ axis is also marked. The dashed gray line $[\Delta\rho(z)]$ exhibits, from left to right, (i) a negative peak associated with electron depletion from the rear side of DMS, (ii) a small positive peak associated with electron accumulation in the region of the sulfur and carbon atoms of DMS, (iii) a negative peak associated with electron depletion from the front side of DMS (involving both the sulfur and the two hydrogen atoms engaged in the hydrogen bonds), and (iv) two positive peaks associated with electron accumulation on the front and rear side of $SO_2$, interleaved by a very small negative peak associated with electron depletion in a narrow region encompassing the $SO_2$ molecular plane.

The CD function, whose value at each $z$ equals the signed area bounded by $\Delta\rho(z)$ from $-\infty$ up to that $z$, is negative along the whole molecular region, thus indicating a $z$-resolved net flow of electrons always in the left-to-right (DMS → $SO_2$) direction. [It is worth recalling here that, by definition, positive values of $\Delta q(z)$ quantify a charge flow from right to left, i.e., the direction of decreasing $z$,

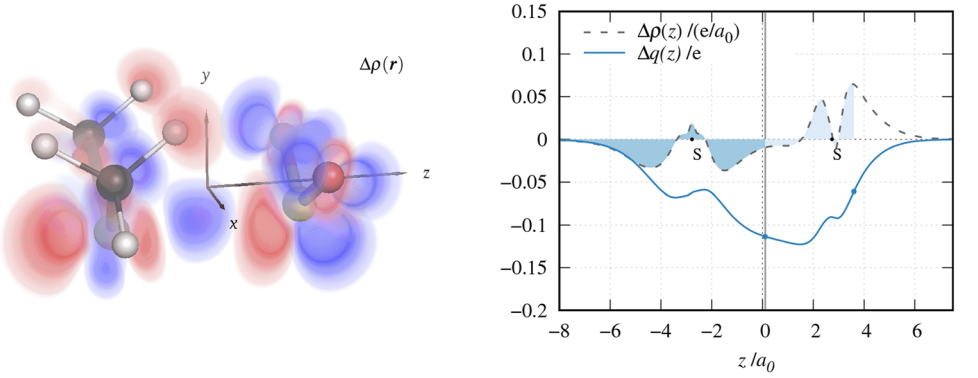


**FIG. 2.** Overall charge redistribution $\Delta\rho(\boldsymbol{r})$ [isosurface layers between $\pm 0.005$ $(e/a_0^3)$, red: electron depletion, blue: electron accumulation] upon binding of DMS to $SO_2$, and associated charge-redistribution profile $\Delta\rho(z)$ and CD function $\Delta q(z)$.

while negative values quantify a charge flow in the opposite direction.] To aid the reader in visually grasping the meaning of the CD function, for two of its points (marked as blue dots on the related curve), the relation with $\Delta\rho(z)$ is made explicit: The first point indicated along the $\Delta q(z)$ curve quantifies the (signed) area bounded by $\Delta\rho(z)$ from $-\infty$ up that $z$, which is filled with the darker blue color, while the second indicated point quantifies the signed area bounded by $\Delta\rho(z)$ from $-\infty$ up to the related $z$ point and filled with the lighter blue color. It is worth noting here that the CD function $\Delta q(z)$ [as well as $\Delta\rho(z)$] goes to zero for $z \to \infty$, meaning that, as expected, the overall molecular charge is conserved upon the intermolecular interaction.

Now, by fixing a plausible dividing $xy$ plane between the fragments, an estimate of the net charge transfer between the fragments can be obtained by taking the value of $\Delta q(z)$ at the $z$ point identifying such plane. A suitable choice for this $z$ point is where equal-valued isodensity surfaces of the electron densities of the two isolated fragments [$\rho^{A}(\boldsymbol{r})$ and $\rho^{B}(\boldsymbol{r})$ of Eq. (1)] become tangent. Such a $z$ point is called the "isoboundary," $z_{ib}$, and is marked by a gray vertical line in Fig. 2. For the herein considered case, the isoboundary is $z_{ib} = 0.1a_0$ and the value of the CD function at the isoboundary is 0.114 $e$, thus indicating a net charge transfer of about 0.11 $e$ from DMS to $SO_2$. Note that this value is slightly lower than that reported in Ref. 18 (0.12 $e$) owing to slight differences in the definition of the reference density describing the unbound fragments, which is a superposition of the simple electron densities of the isolated fragments here [see Eq. (1)], while it involves a preliminary orthogonalization of the fragment orbitals in the NOCV-CD scheme adopted in Ref. 18.

As evident, ordinary CD analysis offers a clear and compact quantitative picture of the charge flow along the interaction axis $z$ occurring upon binding of DMS to $SO_2$, and of the associated net charge transfer between the fragments. However, it provides no way of discerning neither qualitatively nor quantitatively the role of the individual charge flows associated with each of the three interactions present in DMS–$SO_2$ and highlighted in Fig. 1, as they get inevitably mixed upon the integration in Eqs. (2) and (3). This is where LCD analysis comes into play.

### 2. Targeting the sulfur–sulfur interaction

Leveraging on the partitioning scheme described in Sec. II, we might attempt a first partition of the molecule so as to isolate the charge-redistribution component associated with the sulfur–sulfur interaction from the rest. Accordingly, we group the atoms in a subset S–S containing the two sulfur atoms, and in another one $[(CH_3)–O]_2$ containing the remaining atoms, calculate the weight function $w_I(\boldsymbol{r})$, and use this weight function to evaluate the local charge redistribution $\Delta\rho_I(\boldsymbol{r})$ and the CD function $\Delta q_I(z)$ related to each of the two portions of the molecule. The resulting two local charge redistributions for the S–S and $[(CH_3)–O]_2$ portions of the complex are shown in the bottom and top (respectively) left panel of Fig. 3, while the associated CD functions are shown as solid blue line and dashed blue line (respectively) in the right panel of the same figure.

As the two molecular portions include all atoms of the molecule and each atom only appears in one of the two portions, the two curves sum up to the total $\Delta q(z)$, which is also shown for reference as gray solid line in Fig. 3.

The graphical representations of the local charge redistributions (left panel) show that the Hirshfeld partitioning of the overall charge redistribution leads to local contributions which clearly describe the local charge flows relating to the two selected portions of the molecule. Focusing now on their quantitative analysis (right panel), the related CD curves are—as expected—negative in the bonding region, thus both indicating a charge flow in the DMS $\to$ $SO_2$ direction. However, a first apparently puzzling eye-catching feature is that they do not go to zero as $z \to \infty$ but tend to the same absolute value appearing with opposite sign in the two curves. This means that there is no balance in the electron loss and gain described by each of the two curves. Focusing, for instance, on the S–S local charge redistribution, the related CD function tends to $-0.019$ $e$, meaning that the associated charge flow features a defect of charge due to electron-charge migration toward regions of the molecule other than the two sulfur atoms. Arguably, this is due to the fact that, as charge was transferred from the sulfur atom of DMS to the sulfur atom of $SO_2$, the latter atom became a better donor,

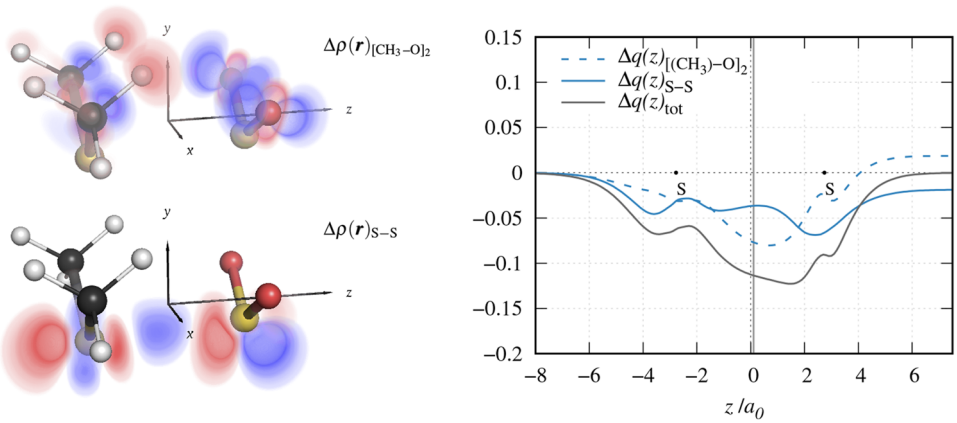


**FIG. 3.** Additive charge-redistribution components [isosurface layers between $\pm 0.005$ ($e/a_0^3$)] and CD functions associated with the $[(CH_3)–O]_2$ and S–S portions of the complex.

**TABLE I.** Values of $\Delta q(z)$ at the so-called isoboundary ($z_{ib} = 0.1a_0$ in the present case) and at $z = \infty$ for the overall CD function ("tot") and its local components S–S, $[CH_3–O]_2$, the two CH–O, and $[H]_4$ displayed in Figs. 2–4.

| | $\Delta q(z = z_{ib})$ $(e)$ | $\Delta q(z = \infty)$ $(e)$ |
|---|---|---|
| Tot | −0.114 | 0.000 |
| S–S | −0.037 | −0.019 |
| $[CH_3–O]_2$ | −0.077 | 0.019 |
| CH–O | −0.025 | 0.023 |
| CH–O | −0.025 | 0.023 |
| $[H]_4$ | −0.027 | −0.027 |

thus inducing an intramolecular charge shift toward the O atoms. As already mentioned, the amount of the transferred charge can be inferred by the value of the CD function at the so-called isoboundary, which coincides with $z = 0.1a_0$ in the present case (gray vertical line in Fig. 3). Accordingly, the charge depleted by the sulfur atom of DMS amounts to 0.037 $e$. However, as just discussed, only a fraction of this amount equal to 0.037 − 0.019 = 0.018 $e$ is found on the sulfur atom of $SO_2$. Note that, for the reader's convenience, the values of $\Delta q(z = z_{ib})$ and $\Delta q(z = \infty)$ for all the CD functions computed for the DMS–$SO_2$ system are summarized in Table I.

Looking now at the $[(CH_3)–O]_2$ curve, this describes a charge transfer $\Delta q(z = z_{ib})$ of 0.077 $e$ from the methyl groups of DMS to the oxygen atoms of $SO_2$, on which an additional fraction $\Delta q(z = \infty)$ of 0.019 $e$ is found.

Summing up, these results suggest that the net DMS → $SO_2$ charge transfer of 0.114 $e$ is partitioned in 0.077 $e$ deriving from the methyl groups of DMS and 0.037 $e$ deriving from the sulfur atom of DMS and that a peculiar feature of the interaction is an intramolecular charge shift from the sulfur to the oxygen atoms of $SO_2$.

### 3. Disentangling the two hydrogen bonds

In order to illustrate the flexibility of the LCD analysis scheme, in this section, we further push the decomposition to isolate from the rest of the molecule each CH···O hydrogen bond. Accordingly, we further partition the previously defined $[CH_3–O]_2$ local charge redistribution in the following three additive components: two relating to the two portions of the molecule containing the atoms involved in each hydrogen bond, both of which we shall label CH–O, and one relating to a collective portion grouping altogether the remaining four hydrogen atoms, which we shall label $[H]_4$.

The associated local charge redistributions are shown in the left panel of Fig. 4 (the two CH–O contributions at the top and center, and the $[H]_4$ one at the bottom).

The first two of these clearly isolate the two equivalent charge flows localized on the two hydrogen bonds, while the last one depicts a minor contribution to the overall charge rearrangement mainly involving charge depletion from the two hydrogens aligned with the hydrogen bonds. The CD function related to this $[H]_4$ component (shorter-dashed blue line in the right panel) reaches a plateau of −0.027 $e$ shortly before the isoboundary ($z_{ib} = 0.1a_0$), meaning that from that $z$ point onward, the charge depletion from the four hydrogen atoms has been completed. On the other hand, the two superimposed curves relating to the CH–O local charge flows (longer-dashed and dotted blue lines) suggest that no significant net electron gain or loss is occurring around the carbon atoms (the curves are flat and very close to zero up to about 1 $a_0$ past the sulfur atom of DMS, at $z \approx -1.8\ a_0$). A visual inspection of the charge redistribution around the carbon atoms of DMS in Fig. 4 reveals indeed that these atoms are mostly concerned with an intra-atomic reorganization involving charge shift from the $sp^3$ orbital directed toward the sulfur atom to the $sp^3$ orbital directed toward the hydrogen atom involved in the hydrogen bond (this is more clearly visible in the top left panel of Fig. 4, showing the local charge redistribution of the CH···O bond lying in the negative-$x$ region). On the contrary, the charge transfer from the hydrogen atoms facing $SO_2$ to the oxygen atom of this fragment amounts to 0.025 $e$ for each hydrogen. The two curves at $z = \infty$ reach a plateau of 0.023 $e$, meaning that the two CH–O local charge redistributions include a fraction of electron charge amounting to 0.023 $e$ flowing in from other, external portions of the molecule. In fact, as already mentioned in Sec. IV A 2, each oxygen receives 0.019/2 = 0.0095 $e$ from the sulfur atom of $SO_2$, plus, as just discussed when commenting the $[H]_4$ CD function, an additional contribution of 0.027/2 = 0.0135 $e$ from the hydrogen atoms

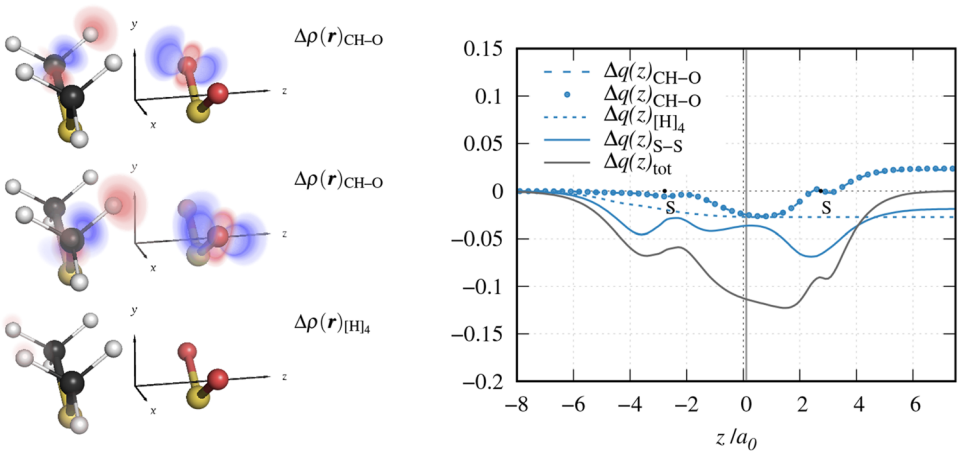


**FIG. 4.** Left panel: decomposition of the charge redistribution of the $[(CH_3)–O]_2$ portion of the complex in further localized terms [isosurface layers between ±0.005 $(e/a_0^3)$] relating to each hydrogen bond (CH–O) and to the remaining H quadruple ($[H]_4$). Right panel: decomposition of the overall CD function in terms of the two CH–O, the $[H]_4$, and the S–S additive partial charge flows.

not directly involved in the respective hydrogen bonds, for a total amount of 0.023 *e*.

For a better assessment of the above discussed results, we performed a Natural Bond Orbital (NBO) analysis[35] on the DMS–$SO_2$ complex and on its isolated DMS and $SO_2$ constituents for the purpose of obtaining NBO atomic charges and calculating the charge loss/gain on each atom (the results were obtained through the same software and level of theory specified in Sec. III and are fully reported in the supplementary material). According to NBO analysis, upon the DMS–$SO_2$ interaction, the sulfur atom of DMS loses 0.055 *e*, and its hydrogen atoms involved in the hydrogen bonds lose 0.028 *e* each. The remaining four hydrogen atoms lose on the whole 0.032 *e*, while the oxygen atoms of $SO_2$ gain 0.066 *e* each. On the other hand, no significant changes are found on the carbon atoms of DMS (electron gain of 0.005 *e*) and on the sulfur atom of $SO_2$ (electron loss of 0.001 *e*). With the exception of the charge change on this last atom (for which our results indicate a small charge accumulation), the NBO results compare reasonably well on a quantitative level with the above discussed ones obtained by LCD analysis despite the difference in spirit of the two methodologies.

## B. Multiple hydrogen bonding in the acetic acid dimer and in DNA base pairs

Among the most iconic intermolecular interactions in chemistry and biology are those involved in DNA base-pairing. As is known, these interactions involve parallel concurrent charge flows arising from multiple hydrogen bonding between the adenine–thymine (A–T) and guanine–cytosine (C–G) base pairs. As a result, also in this case, ordinary CD analysis would return an averaged picture of the multiple charge flows and no detailed information on each of them. In this section, we will apply the analysis LCD scheme to quantitatively characterize the charge flows associated with each hydrogen bond in both the A–T and C–G systems. In a first stage, however, it will be beneficial to carry out a preliminary analysis on some aspects related to charge transfer in the hydrogen bonds of simpler chemical systems.

### *1. Hydrogen bonding in simpler chemical contexts*

The analysis in Sec. IV A on the interaction between DMS and $SO_2$ revealed that the charge redistribution localized around the two CH···O hydrogen bonds involves a DMS → $SO_2$ charge transfer in the direction from the hydrogen-bond donor to the hydrogen-bond acceptor. This is in contrast with the widely accepted view that hydrogen bonding typically involves a small amount of charge transfer (0.01–0.03 *e*) from the proton-acceptor to the proton-donor molecule.[36] Before analyzing base-pairing interactions in DNA, this aspect is worth being further examined. For this purpose, we shall here consider hydrogen bonding in the much simpler chemical contexts of the water dimer and of the acetic acid dimer.

The water dimer is a very simple system that can be conveniently treated with ordinary CD analysis by choosing the $z$ axis as the one joining the two oxygen atoms. The results of such analysis on this system are collected in Fig. 5, where the overall charge redistribution $\Delta\rho(\boldsymbol{r})$ upon the interaction, and the associated charge-redistribution profile $\Delta\rho(z)$ and CD function $\Delta q(z)$, are reported.

The CD function (right panel) is always negative, indicating a $z$-resolved flow of electrons always in the left-to-right direction, i.e., the direction from the hydrogen-bond acceptor to the hydrogen-bond donor. Such flow results from a charge shift that originates around the two hydrogen atoms bound to the proton-acceptor oxygen, where electron depletion is found, and terminates on the rear side of the proton-donor oxygen and on the hydrogen atom bound to this oxygen, where electron accumulation is found. Moreover, an eye-catching feature of the overall charge redistribution is the red lobe on the hydrogen atom involved in the hydrogen bond, which indicates charge depletion on this hydrogen. Such charge depletion is indeed a known feature of hydrogen bonding [see criterion (5) in Ref. 37], further confirmed by the fact that NMR shifts show that protons involved in hydrogen bonding are descreened. As already mentioned, a clear-cut estimate of the charge transfer between the fragments upon their interaction is provided by the value of the CD function at the isoboundary, $\Delta q(z = z_{ib})$, with $z_{ib} = 2.4a_0$ for the present case. Accordingly, hydrogen bonding in the considered water dimer involves a charge transfer of 0.014 *e* from the proton-acceptor to the proton-donor fragment. These results, which are fully consistent, both qualitatively and quantitatively, with those obtained using the same methodology by other authors in Ref. 38, are perfectly in line with the above mentioned widely accepted view that hydrogen bonding involves a small amount of charge transfer from the proton-acceptor to the proton-donor molecule.

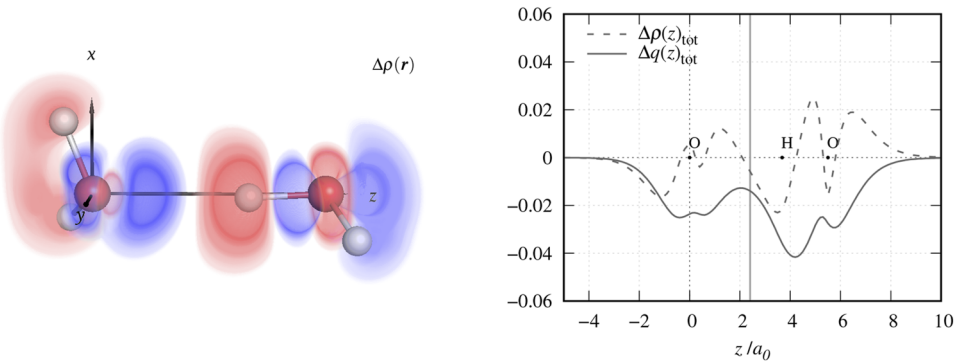


**FIG. 5.** Overall charge redistribution $\Delta\rho(\boldsymbol{r})$ [isosurface layers between $\pm 0.0025$ $(e/a_0^3)$] upon hydrogen bonding in the water dimer, and associated charge-redistribution profile $\Delta\rho(z)$ and CD function $\Delta q(z)$.

The above outlined picture, however, changes considerably if we now move to the slightly more complex case of the acetic acid dimer, featuring two parallel O···HO and OH···O hydrogen bonds running in opposite directions, which cannot be independently analyzed with ordinary CD analysis. We thus applied LCD analysis on this system in order to isolate the two local charge-redistribution components related to each hydrogen bond. For this purpose, with reference to the molecular structure displayed in the left panel of Fig. 6, we partitioned the molecular system in two portions divided by the *yz* plane: one ("d2") containing the H and O atoms with positive *x* coordinate and one ("d1") containing the H and O atoms with negative *x* coordinate. We then assigned the four C atoms lying on the *z* axis to both portions in equal share by halving their Hirshfeld weight used for their inclusion in both portions of the molecule. The results of LCD analysis on this system are summarized in Fig. 6, where the overall charge-redistribution and its local components related to the two hydrogen bonds are reported together with the associated CD functions (vertical dashed lines mark the isoboundary for each hydrogen bond).

In this case, while the qualitative pattern of the local charge redistribution on each hydrogen bond closely resembles that featured by the water dimer (with a depletion region on the hydrogen atom sandwiched by charge-accumulation regions), the CD functions unequivocally indicate a charge transfer in the opposite direction, i.e., from the proton-donor to the proton-acceptor fragment. The null net charge transfer between the fragments (value of the total CD function midway between the two marked isoboundaries) results indeed from identical charge flows running in opposite directions and featuring a CT of 0.042 *e* in the direction from the proton-donor to the proton-acceptor oxygen. More in detail, focusing on the "d2" hydrogen bond, which features the same O···HO spatial disposition as the hydrogen bond of the water dimer analyzed in Fig. 5, one immediately sees that while the CD curve in the O···H segment is negative for the water dimer (indicating charge flow from left to right), it is indeed positive for the acetic acid dimer (indicating charge flow from right to left), arguably owing to the different chemical context and orbital hybridization of the involved oxygen atoms.

To double check the dependence of these results on the specific adopted definition of the molecular portions, we extended the analysis to three further possible apportionments of the acetic acid dimer (essentially grouping the carbon atoms with the two hydrogen bonds in different ways). The results, which are fully detailed in the supplementary material together with additional plots also showing the charge-redistribution profile $\Delta\rho(z)$ for a direct comparison with that of the water dimer in Fig. 5, confirm in all four cases a charge flow in the direction from the proton-donor to the proton-acceptor oxygen, with the extent of the charge transfer ranging between 0.030 and 0.046 *e*.

### 2. Adenine–thymine

As is known, base-pairing in the A–T molecular system is due to two concurrent hydrogen bonds, NH···N and O···HN, running in parallel and involving charge flows in opposite directions (see Fig. 7). We, thus, computed the overall charge redistribution upon binding of A to T, and applied LCD analysis to disentangle the local components relating to each of the two hydrogen bonds, plus the residual part of the charge redistribution. These three local components are shown in the left panel of Fig. 7, labeled as NH–N, O–HN, and "res," respectively.

The two NH–N and O–HN charge-redistribution components exhibit a charge depletion/accumulation pattern very similar to that featured by the hydrogen bonds in the acetic acid dimer, with charge depletion on the hydrogen atom flanked by charge-accumulation regions. The last component mainly depicts charge rearrangement around the carbon atoms bound to the hydrogen-bond donors/acceptors plus significant electron depletion from the H atom of adenine with highest *y* coordinate.

Turning now to the quantitative characterization of these local charge flows, the related CD functions are plotted in the right panel of Fig. 7, where also the CD function associated with the overall charge redistribution is shown for reference. Also, in this case, a reference frame aligned with the principal axes of inertia is a well-suited one for defining an interaction axis *z* that runs parallel to the two main interactions. In the same plot, a gray vertical line marks the isoboundary, here defined—more appropriately—as the *z* point

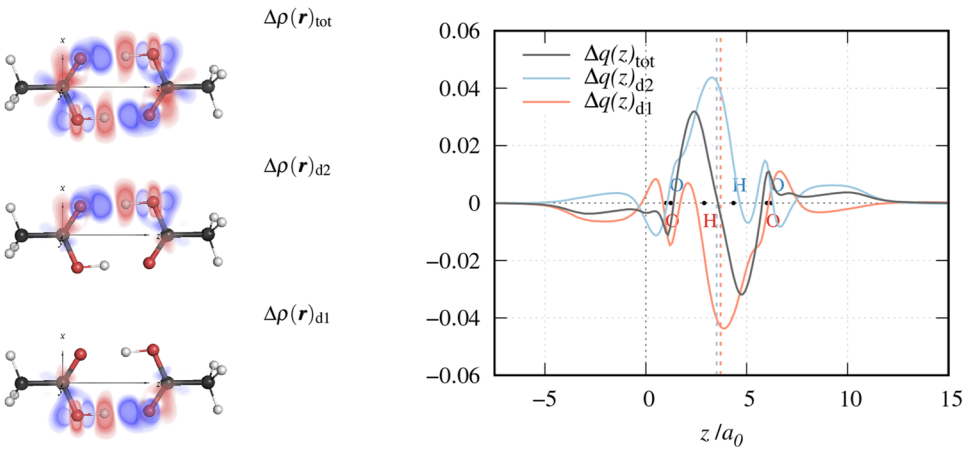


**FIG. 6.** Overall charge-redistribution and its local components [isosurface layers between ±0.005 ($e/a_0^3$)] related to the two hydrogen bonds in the acetic acid dimer, together with the associated CD functions.

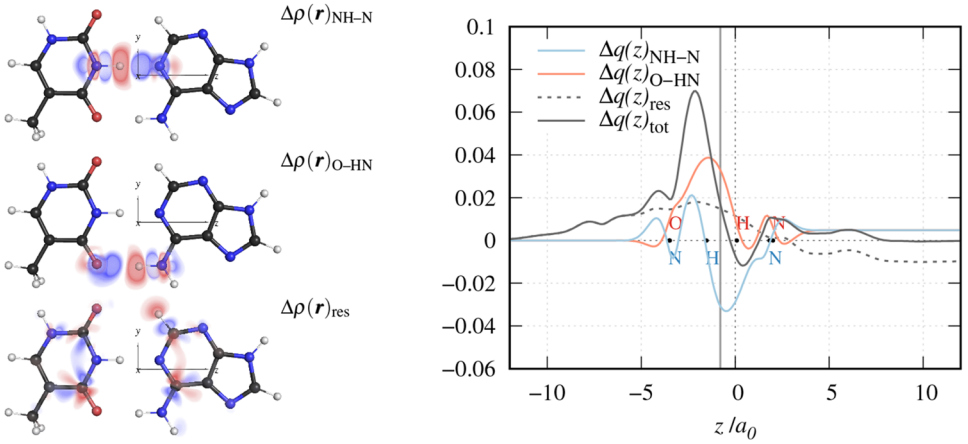


**FIG. 7.** Additive charge-redistribution components [isosurface layers between $\pm 0.0025\ (e/a_0^3)$] and CD functions associated with the two hydrogen bonds (NH–N and O–HN) and with the residual portion of the molecule ("res") in the A–T base pair.

where the planar densities (see Sec. II) of the fragments intersect, so as to account in an averaged way for the multiple "contact" points between the fragments, leading to $z_{\mathrm{ib}} = -0.8a_0$.

The NH–N (light blue) curve features a large negative peak in the H–N region, corresponding to charge flow in the NH → N direction, while the O–HN (light red) curve features a large positive peak in the O–H region, corresponding to charge flow in the O ← HN direction. The curve relating to the residual charge redistribution (dashed gray) describes charge flow in the T ← A direction up to $z \approx 2a_0$ and charge flow in the opposite direction for higher values of $z$. The charge gain/loss balance, however, is not perfect in the three curves. In particular, judging from the plateau of the three curves (0.005, 0.005, and −0.010 $e$, respectively), a charge fraction of 0.010 $e$ is found to flow from the atoms of the residual region to those involved in the two hydrogen bonds, and such fraction is equally distributed among the two interactions. Finally, a net T ← A charge transfer of 0.017 $e$ from is observed, resulting from NH–N, O–HN, and "res" contributions of −0.031, 0.033, and 0.015 $e$, respectively.

The above outlined picture is in line with results obtained by other authors using different methodologies. In particular, both Refs. 39 and 40, based, respectively, on Voronoi Deformation Density (VDD) analysis and on Bader's theory of Atoms in Molecules (AIM), indicate a net charge transfer from A to T. The reported values (0.03 and 0.035 $e$, respectively) are slightly higher than that obtained by LCD analysis, likely due to the fact that in LCD analysis the isoboundary operates an approximate separation (through a dividing plane) between the interacting fragments, while a more accurate choice could be the definition of an isoboundary for each of the two hydrogen bonds. Focusing now on the in-depth picture relating to each hydrogen bond, our results are fully compatible with the outcome of the charge-redistribution analysis reported in Ref. 39, whereby electron loss is found on the hydrogen atoms involved in the hydrogen bonds, while a charge gain of 0.031 and of 0.037 $e$ is found on the proton-acceptor N atom of A and on the proton-acceptor O atom of T, respectively.

### 3. Guanine–cytosine

LCD analysis was also applied on the analogous C–G system, and the results are for illustrative purposes summarized in Fig. 8.

Base-pairing here results from three concurrent hydrogen bonds, labeled O–HN, N–HN, and NH–O in the figure, plus a residual charge redistribution labeled "res." These local components of the overall charge redistribution are shown in the left panel of Fig. 8, while the related CD functions are plotted in the right panel of the same figure. The overall picture is similar to that of the A–T system, with the curves relating to the three hydrogen bonds quantitatively describing focused charge flows running in opposite directions. On the contrary, the CD function associated with the charge redistribution on the residual portion of the molecule is here always negative and thus describes a charge flow always in the left to right (C → G) direction. Another interesting feature here is that the four local components are virtually independent one from another, as they all approximately tend to zero as $z \to \infty$. In particular, in contrast with its counterpart in the A–T system, the "res" component here features a perfect balance of charge gain/loss, probably owing to the fact that, in contrast with A–T, no hydrogen atom bound to one of the carbon atoms contiguous to the hydrogen bonds is here available for charge withdrawal.

## C. Ambifunctional hydrogen bond in ammonia–pyridine

As a final example, we turn our attention to the interesting case of the ammonia–pyridine complex. This complex, which was computationally and experimentally characterized in Ref. 33, exhibits the challenging feature of so-called ambifunctional hydrogen bonding.[41]

A visual inspection of Fig. 9, showing the overall charge redistribution associated with the interaction of the two fragments, reveals in fact that the interaction is due to a NH···N hydrogen bond and to a N···HC hydrogen bond, both featuring (though the second one less distinctively) charge depletion on the hydrogen atoms sandwiched by charge-accumulation regions (see the charge-accumulation region around the N atom of ammonia extending also toward the hydrogen atom involved in the N···HC hydrogen bond). In trying to dissect the overall interaction in its main components, this situation is particularly challenging due to the fact that the same N atom of ammonia is involved in both the above-mentioned hydrogen bonds.

In approaching this complex, we firstly attempted a tentative partition isolating the NH···N hydrogen bond, the adjacent

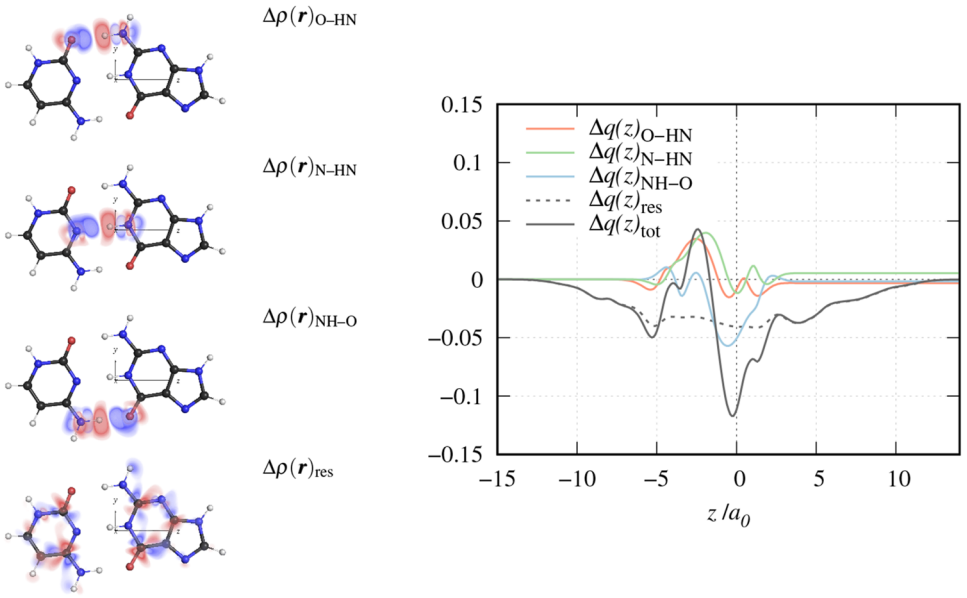


**FIG. 8.** Additive charge-redistribution components [isosurface layers between $\pm 0.0025$ ($e/a_0^3$)] and CD functions associated with the three hydrogen bonds (O–HN, N–HN, and NH–O) and with the residual portion of the molecule ("res") in the C-G base pair.

HC group (involved in the second hydrogen bond), and the residual portion of the molecule. The results of LCD analysis based on this partition are summarized in Fig. 10, showing the local charge-redistribution components in the left panel and the related CD functions in the right panel.

Also, in this case, a suitable reference frame is that of the principal axes of inertia, where the $z$ axis well represents the interaction axis between the two interacting fragments (the isoboundary, here computed in the same way as for the A–T system, i.e., as the $z$ point of intersection between the fragments' planar densities, is $z_{\text{ib}} = -4.0a_0$). An analysis of the results summarized in Fig. 10, however, suggests that such apportionment of the molecular regions is inadequate to properly characterize the interaction. In fact, the NH···N hydrogen bond seems poorly described, featuring an almost null charge transfer (the value of the CD function at $z = z_{\text{ib}}$ is $-0.004$ $e$), while the second hydrogen bond is not characterized at all, as the second portion of the molecule only focuses on the HC group. Finally, LCD analysis on the "res" portion reveals that a fraction of about 0.01 $e$ accumulates, upon the interaction, on the H atoms of ammonia not involved in hydrogen bonding.

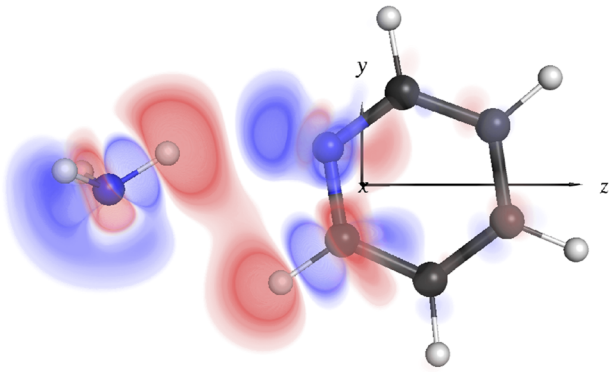


**FIG. 9.** Overall charge redistribution $\Delta\rho(\boldsymbol{r})$ [isosurface layers between $\pm 0.001$ ($e/a_0^3$)] upon binding of ammonia to pyridine.

Arguably, a better description of this intermolecular interaction could be obtained by allowing the same N atom, or—even better—the $H_2N$ group of ammonia with the two hydrogens being those not involved in the hydrogen bond, to be simultaneously present in different portions of the molecule accounting for the two NH···N and N···HC hydrogen bonds. With this in mind, and with aim of preserving the additivity of the LCD curves, we proceeded as follows: With reference to the molecular geometry of the system displayed in Fig. 9, we divided the pyridine molecule in a first part containing all atoms with positive $y$ coordinate and a second part containing all atoms with negative $y$ coordinate. To the first part, we also added the H atom of ammonia involved in the NH···N hydrogen bond. Then, we included the remaining $H_2N$ fragment in both portions of the molecule but with different weight. In other words, we further weighed the Hirshfeld weight functions of these three atoms with a weight coefficient $c_1$ for the first part and $c_2$ for the second part such that $c_1 + c_2 = 1$. We then performed an heuristic search of those precise values of $c_1$ and $c_2$ that made the CD curves associated with the two portions of the molecule tend to zero for $z \to \infty$, leading to $c_2 = 0.95$ and $c_1 = 0.05$.

While this procedure may seem somewhat intricate and arbitrary, it nonetheless leads to a compact picture of the interaction summarized by the results reported in Fig. 11.

In so doing, in fact, the overall charge redistribution upon binding of ammonia to pyridine is partitioned in two "independent" components (in the sense that each component describes charge-conserving electron flows) clearly localized on the two (NH···N and N···HC) hydrogen bonds. The associated curves show that the almost null overall charge transfer between the fragments [the value

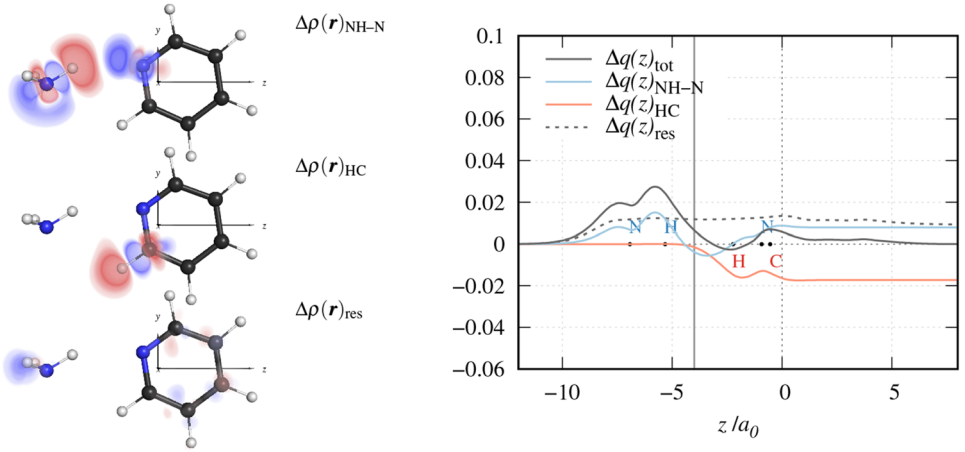


**FIG. 10.** Additive charge-redistribution components [isosurface layers between $\pm 0.001$ $(e/a_0^3)$] and CD functions associated with the NH···N hydrogen bond (NH–N), with the adjacent HC group (HC), and with the residual portion of the molecule ("res") in the ammonia–pyridine complex.

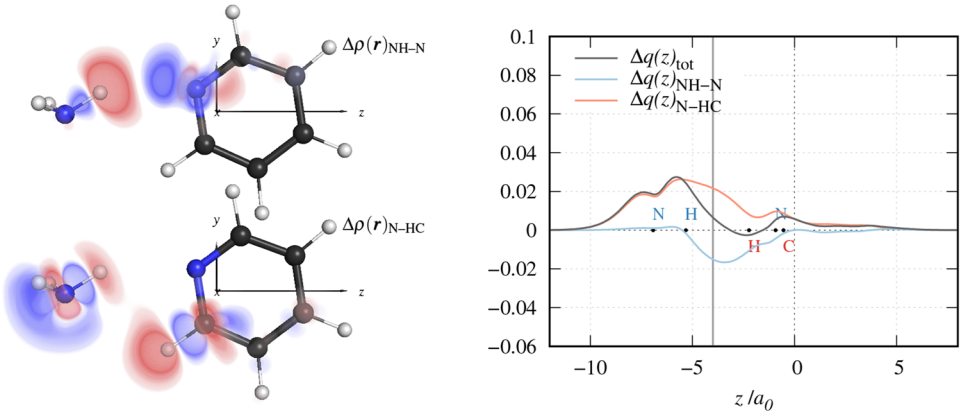


**FIG. 11.** Decomposition of the charge redistribution [isosurface layers between $\pm 0.001$ $(e/a_0^3)$] upon binding of ammonia to pyridine in two additive components (see text for their definition) relating to the primary (NH–N) and secondary (N–HC) hydrogen bonds, both involving the same N atom of ammonia.

of the $\Delta q(z)_{\mathrm{tot}}$ CD function at the isoboundary is 0.007 $e$] results from an ammonia → pyridine transfer of 0.015 $e$ associated with a charge flow localized on the NH···N interaction and from an ammonia ← pyridine transfer of 0.022 $e$ associated with a charge flow localized on the N···HC interaction.

## V. CONCLUSIONS AND PERSPECTIVES

This article reports on a novel analysis scheme for a quantitative characterization of local charge flows in complex intermolecular interactions. The scheme couples a Hirshfeld partitioning of the charge redistribution occurring around two molecular fragments upon their mutual interaction to the charge-displacement (CD) analysis which provides a clear and compact picture of charge-flow profiles along a given interaction axis. In the resulting local charge-displacement (LCD) analysis scheme, the molecular system is partitioned in several portions relating to relevant components of the overall interaction, and the associated partial additive contributions to the overall charge redistribution are computed and quantitatively analyzed one at a time. While the proposed methodology shares with the original Hirshfeld partitioning scheme a certain degree of arbitrariness, some of the shortcomings of Hirshfeld's scheme can be overcome by an easy integration of more refined Hirshfeld partitioning approaches.[26,27]

The features of the method were illustrated and assessed through test calculations on a simple yet interesting system, the DMS–$SO_2$ complex, where a homochalcogen bond and a pair of hydrogen bonds concur in the overall interaction. By means of LCD analysis, the charge flows related to these different interactions were filtered out from the overall charge redistribution and quantitatively characterized. The analysis was then extended to hydrogen bonding in the acetic acid dimer and to base-pairing interactions in DNA, where individual charge flows of the multiple hydrogen bonds involved in the pairing of adenine and thymine and of guanine and cytosine could be quantitatively characterized. Additionally, LCD analysis was performed on the challenging case of the ammonia–pyridine complex, featuring ambifunctional hydrogen bonding. The obtained results offer new insight from the unprecedented perspective of CD analysis on aspects related to charge transfer in hydrogen bonding across different chemical contexts, highlighting, in some cases, an unexpected behavior and prompting for a more systematic investigation, which we have presently undertaken and which will be the subject of future work.

The developed scheme can easily be integrated in the several existing flavors of CD analysis, i.e., the NOCV-CD method,[8,9] the

curvilinear CD analysis,[20] and CD analysis in the relativistic framework.[9] Moreover, the integration of the LCD analysis scheme with state-of-the-art immersive-virtual-reality technology in the virtual laboratory for the analysis of chemical bonding recently developed in our group[42,43] is also easily achievable and work is ongoing in this respect.

Summing up, the devised methodology extends the applicability of CD analysis to a new, interesting class of systems featuring complex intermolecular interactions resulting from multiple charge flows, thus allowing for the exploitation of the potentialities of CD analysis in so far unexplored contexts. Future directions in an applicative context may, for instance, regard the in-depth characterization of the so-called "spodium bond," a term that has been recently proposed to describe the non-coordinative interaction that can be established between a polarized group 12 metal and a mild Lewis base.[44] Most of the systems showing short metal-donor distances compatible with spodium bonding are in fact characterized by the coexistence of multiple weak interactions, including hydrogen and halogen bonding, making the assessment of the real importance of the spodium bond difficult,[45] and LCD analysis may reveal a versatile tool for a thorough characterization of the intermolecular interactions in these systems.

## SUPPLEMENTARY MATERIAL

See the supplementary material for an analysis of alternative definitions of the interaction axis in DMS–$SO_2$, for additional results on DMS–$SO_2$, on the acetic acid dimer and on the A–T base pair, and for the molecular geometries of the systems considered in the article.

## ACKNOWLEDGMENTS

The research leading to these results has received funding from Scuola Normale Superiore through projects "LCFA—Local charge-flow analysis: a novel scheme for unraveling complex intermolecular interactions" (Grant No. SNS21_A_RAMPINO) and "DIVE: Development of Immersive approaches for the analysis of chemical bonding through Virtual-reality Environments" (Grant No. SNS18_B_RAMPINO), and program "Finanziamento a supporto della ricerca di base" (Grant No. SNS_RB_RAMPINO). The results were obtained through a parallel computer code partly developed within the Project HPC-EUROPA3 (Grant No. INFRAIA-2016-1-730897), with the support of the EC Research Innovation Action under the H2020 Program. S.R. gratefully acknowledges the support of Professor Carole Morrison of the School of Chemistry of the University of Edinburgh and the computer resources and technical support provided by the Edinburgh Parallel Computing Centre.

## AUTHOR DECLARATIONS

### Conflict of Interest

The authors have no conflicts to disclose.

### Author Contributions

**G. Nottoli**: Conceptualization (supporting); Data curation (equal); Formal analysis (equal); Investigation (lead); Software (lead); Validation (equal); Visualization (equal); Writing – review & editing (supporting). **B. Ballotta**: Data curation (lead); Formal analysis (equal); Investigation (lead); Validation (lead); Writing – original draft (supporting). **S. Rampino**: Conceptualization (lead); Formal analysis (equal); Funding acquisition (lead); Methodology (lead); Project administration (lead); Resources (lead); Software (equal); Supervision (lead); Visualization (equal); Writing – original draft (lead); Writing – review & editing (lead).

## DATA AVAILABILITY

The data that support the findings of this study are available from the corresponding author upon reasonable request.

## REFERENCES

[1] G. N. Lewis, "The atom and the molecule," J. Am. Chem. Soc. **38**, 762–785 (1916).
[2] R. F. W. Bader, W. H. Henneker, and P. E. Cade, "Molecular charge distributions and chemical binding," J. Chem. Phys. **46**, 3341–3363 (1967).
[3] R. F. W. Bader, I. Keaveny, and P. E. Cade, "Molecular charge distributions and chemical binding. II. First-row diatomic hydrides, AH," J. Chem. Phys. **47**, 3381–3402 (1967).
[4] R. E. Brown and H. Shull, "A configuration interaction study of the four lowest $^1\Sigma^+$ states of the LiH molecule," Int. J. Quantum Chem. **2**, 663–685 (1968).
[5] P. Politzer and R. R. Harris, "Properties of atoms in molecules. I. Proposed definition of the charge on an atom in a molecule," J. Am. Chem. Soc. **92**, 6451–6454 (1970).
[6] L. Belpassi, I. Infante, F. Tarantelli, and L. Visscher, "The chemical bond between Au(I) and the noble gases. Comparative study of NgAuF and $NgAu^+$ (Ng = Ar, Kr, Xe) by density functional and coupled cluster methods," J. Am. Chem. Soc. **130**, 1048–1060 (2008).
[7] S. Rampino, *Chemistry at the Frontier with Physics and Computer Science: Theory and Computation* (Elsevier, Amsterdam, 2022).
[8] G. Bistoni, S. Rampino, F. Tarantelli, and L. Belpassi, "Charge-displacement analysis via natural orbitals for chemical valence: Charge transfer effects in coordination chemistry," J. Chem. Phys. **142**, 084112 (2015).
[9] M. De Santis, S. Rampino, H. M. Quiney, L. Belpassi, and L. Storchi, "Charge-displacement analysis via natural orbitals for chemical valence in the four-component relativistic framework," J. Chem. Theory Comput. **14**, 1286–1296 (2018).
[10] G. Bistoni, S. Rampino, N. Scafuri, G. Ciancaleoni, D. Zuccaccia, L. Belpassi, and F. Tarantelli, "How $\pi$ back-donation quantitatively controls the CO stretching response in classical and non-classical metal carbonyl complexes," Chem. Sci. **7**, 1174–1184 (2016).
[11] M. Fusè, I. Rimoldi, E. Cesarotti, S. Rampino, and V. Barone, "On the relation between carbonyl stretching frequencies and the donor power of chelating diphosphines in nickel dicarbonyl complexes," Phys. Chem. Chem. Phys. **19**, 9028–9038 (2017).
[12] M. Fusè, I. Rimoldi, G. Facchetti, S. Rampino, and V. Barone, "Exploiting coordination geometry to selectively predict the $\sigma$-donor and $\pi$-acceptor abilities of ligands: A back-and-forth journey between electronic properties and spectroscopy," Chem. Commun. **54**, 2397–2400 (2018).
[13] M. Schmitt and I. Krossing, "Terminal end-on coordination of dinitrogen versus isoelectronic CO: A comparison using the charge displacement analysis," J. Comput. Chem. (published online 2022).
[14] D. Cappelletti, E. Ronca, L. Belpassi, F. Tarantelli, and F. Pirani, "Revealing charge-transfer effects in gas-phase water chemistry," Acc. Chem. Res. **45**, 1571–1580 (2012).
[15] G. Ciancaleoni, C. Santi, M. Ragni, and A. L. Braga, "Charge-displacement analysis as a tool to study chalcogen bonded adducts and predict their association constants in solution," Dalton Trans. **44**, 20168–20175 (2015).

[16]F. Nunzi, D. Cesario, F. Pirani, L. Belpassi, G. Frenking, F. Grandinetti, and F. Tarantelli, "Helium accepts back-donation in highly polar complexes: New insights into the weak chemical bond," J. Phys. Chem. Lett. **8**, 3334–3340 (2017).
[17]W. Li, L. Spada, N. Tasinato, S. Rampino, L. Evangelisti, A. Gualandi, P. G. Cozzi, S. Melandri, V. Barone, and C. Puzzarini, "Theory meets experiment for noncovalent complexes: The puzzling case of pnicogen interactions," Angew. Chem., Int. Ed. **57**, 13853–13857 (2018).
[18]D. A. Obenchain, L. Spada, S. Alessandrini, S. Rampino, S. Herbers, N. Tasinato, M. Mendolicchio, P. Kraus, J. Gauss, C. Puzzarini, J.-U. Grabow, and V. Barone, "Unveiling the sulfur–sulfur bridge: Accurate structural and energetic characterization of a homochalcogen intermolecular bond," Angew. Chem., Int. Ed. **57**, 15822–15826 (2018).
[19]A. Patti, S. Pedotti, G. Mazzeo, G. Longhi, S. Abbate, L. Paoloni, J. Bloino, S. Rampino, and V. Barone, "Ferrocenes with simple chiral substituents: An in-depth theoretical and experimental VCD and ECD study," Phys. Chem. Chem. Phys. **21**, 9419–9432 (2019).
[20]L. Sagresti and S. Rampino, "Charge-flow profiles along curvilinear paths: A flexible scheme for the analysis of charge displacement upon intermolecular interactions," Molecules **26**, 6409 (2021).
[21]S. Rampino, L. Storchi, and L. Belpassi, "Gold–superheavy-element interaction in diatomics and cluster adducts: A combined four-component Dirac-Kohn-Sham/charge-displacement study," J. Chem. Phys. **143**, 024307 (2015).
[22]M. De Santis, S. Rampino, L. Storchi, L. Belpassi, and F. Tarantelli, "The chemical bond and s-d hybridization in coinage metal(I) cyanides," Inorg. Chem. **58**, 11716–11729 (2019).
[23]S. Rampino, L. Belpassi, F. Tarantelli, and L. Storchi, "Full parallel implementation of an all-electron four-component Dirac-Kohn-Sham program," J. Chem. Theory Comput. **10**, 3766–3776 (2014).
[24]L. Storchi, S. Rampino, L. Belpassi, F. Tarantelli, and H. M. Quiney, "Efficient parallel all-electron four-component Dirac–Kohn–Sham program using a distributed matrix approach II," J. Chem. Theory Comput. **9**, 5356–5364 (2013).
[25]F. L. Hirshfeld, "Bonded-atom fragments for describing molecular charge densities," Theor. Chim. Acta **44**, 129–138 (1977).
[26]P. Bultinck, C. Van Alsenoy, P. W. Ayers, and R. Carbó-Dorca, "Critical analysis and extension of the Hirshfeld atoms in molecules," J. Chem. Phys. **126**, 144111 (2007).
[27]F. Heidar-Zadeh, P. W. Ayers, T. Verstraelen, I. Vinogradov, E. Vöhringer-Martinez, and P. Bultinck, "Information-theoretic approaches to atoms-in-molecules: Hirshfeld family of partitioning schemes," J. Phys. Chem. A **122**, 4219–4245 (2018).
[28]M. J. Frisch, G. W. Trucks, H. B. Schlegel, G. E. Scuseria, M. A. Robb, J. R. Cheeseman, G. Scalmani, V. Barone, G. A. Petersson, H. Nakatsuji, X. Li, M. Caricato, A. V. Marenich, J. Bloino, B. G. Janesko, R. Gomperts, B. Mennucci, H. P. Hratchian, J. V. Ortiz, A. F. Izmaylov, J. L. Sonnenberg, D. Williams-Young, F. Ding, F. Lipparini, F. Egidi, J. Goings, B. Peng, A. Petrone, T. Henderson, D. Ranasinghe, V. G. Zakrzewski, J. Gao, N. Rega, G. Zheng, W. Liang, M. Hada, M. Ehara, K. Toyota, R. Fukuda, J. Hasegawa, M. Ishida, T. Nakajima, Y. Honda, O. Kitao, H. Nakai, T. Vreven, K. Throssell, J. A. Montgomery, Jr., J. E. Peralta, F. Ogliaro, M. J. Bearpark, J. J. Heyd, E. N. Brothers, K. N. Kudin, V. N. Staroverov, T. A. Keith, R. Kobayashi, J. Normand, K. Raghavachari, A. P. Rendell, J. C. Burant, S. S. Iyengar, J. Tomasi, M. Cossi, J. M. Millam, M. Klene, C. Adamo, R. Cammi, J. W. Ochterski, R. L. Martin, K. Morokuma, O. Farkas, J. B. Foresman, and D. J. Fox, GAUSSIAN 16, Revision C.01, Gaussian, Inc., Wallingford, CT, 2016.
[29]S. Grimme, "Semiempirical hybrid density functional with perturbative second-order correlation," J. Chem. Phys. **124**, 034108 (2006).
[30]E. Papajak, H. R. Leverentz, J. Zheng, and D. G. Truhlar, "Efficient diffuse basis sets: cc-pV*x*Z+ and maug-cc-pV*x*Z," J. Chem. Theory Comput. **5**, 1197–1202 (2009).
[31]S. Grimme, J. Antony, S. Ehrlich, and H. Krieg, "A consistent and accurate *ab initio* parametrization of density functional dispersion correction (DFT-D) for the 94 elements H-Pu," J. Chem. Phys. **132**, 154104 (2010).
[32]T. Fornaro, M. Biczysko, J. Bloino, and V. Barone, "Reliable vibrational wavenumbers for C=O and N–H stretchings of isolated and hydrogen-bonded nucleic acid bases," Phys. Chem. Chem. Phys. **18**, 8479–8490 (2016).
[33]L. Spada, N. Tasinato, F. Vazart, V. Barone, W. Caminati, and C. Puzzarini, "Noncovalent interactions and internal dynamics in pyridine–ammonia: A combined quantum-chemical and microwave spectroscopy study," Chem. - Eur. J. **23**, 4876–4883 (2017).
[34]S. Rampino, CUBES: A library and a program suite for manipulating orbitals and densities, VIRT & L-COMM.7.2015.6 (2015).
[35]E. D. Glendening, C. R. Landis, and F. Weinhold, "Natural bond orbital methods," Wiley Interdiscip. Rev.: Comput. Mol. Sci. **2**, 1–42 (2012).
[36]P. Hobza and Z. Havlas, "Blue-shifting hydrogen bonds," Chem. Rev. **100**, 4253–4264 (2000).
[37]U. Koch and P. L. A. Popelier, "Characterization of C–H–O hydrogen bonds on the basis of the charge density," J. Phys. Chem. **99**, 9747–9754 (1995).
[38]E. Ronca, L. Belpassi, and F. Tarantelli, "A quantitative view of charge transfer in the hydrogen bond: The water dimer case," ChemPhysChem **15**, 2682–2687 (2014).
[39]C. Fonseca Guerra, F. M. Bickelhaupt, J. G. Snijders, and E. J. Baerends, "The nature of the hydrogen bond in DNA base pairs: The role of charge transfer and resonance assistance," Chem. - Eur. J. **5**, 3581–3594 (1999).
[40]R. Parthasarathi, R. Amutha, V. Subramanian, B. U. Nair, and T. Ramasami, "Bader's and reactivity descriptors' analysis of DNA base pairs," J. Phys. Chem. A **108**, 3817–3828 (2004).
[41]V. Vennelakanti, H. W. Qi, R. Mehmood, and H. J. Kulik, "When are two hydrogen bonds better than one? Accurate first-principles models explain the balance of hydrogen bond donors and acceptors found in proteins," Chem. Sci. **12**, 1147–1162 (2021).
[42]A. Salvadori, M. Fusè, G. Mancini, S. Rampino, and V. Barone, "Diving into chemical bonding: An immersive analysis of the electron charge rearrangement through virtual reality," J. Comput. Chem. **39**, 2607–2617 (2018).
[43]J. Lupi, M. Martino, A. Salvadori, S. Rampino, G. Mancini, and V. Barone, "Virtual reality tools for advanced modeling," AIP Conf. Proc. **2145**, 020001 (2019).
[44]A. Bauzá, I. Alkorta, J. Elguero, T. J. Mooibroek, and A. Frontera, "Spodium bonds: Noncovalent interactions involving group 12 elements," Angew. Chem., Int. Ed. **59**, 17482–17487 (2020).
[45]G. Ciancaleoni and L. Rocchigiani, "Assessing the orbital contribution in the 'spodium bond' by natural orbital for chemical valence–charge displacement analysis," Inorg. Chem. **60**, 4683–4692 (2021).